Zernike terms including C33 and C42, which were significantly higher in the triplopia group.

Clinically, it is important to know that early nuclear cataract can cause triplopia even when the BCVA is high (Kaufman and Sugar, 1996). In fact, eight out of nine eyes in the triplopia group showed BCVA ≥20/40. All patients underwent cataract surgery based on the evidence obtained from the simulated data of wavefront analysis, and the triplopia disappeared in all cases. Therefore wavefront analysis was very useful for the objective evaluation of eyes with triplopia and for evidence-based ophthalmology.

### Proprietary interest

Yoko Hirohara and Toshifumi Mihashi are employees of Topcon Co.

### Acknowledgements

The authors thank Sayuri Ninomiya and Teruhito Kuroda for the preparation of this study.

This study was supported by a Health Sciences Grant from the Ministry of Health, Labor and Welfare, Japan (H16-Sensory-001), and by a grant from the Ministry of Education, Culture, Sports, Science and Technology (C-2-16591752), Japan (TF).

### References

Bowman, K. J., Smith, G. and Carney, L. G. (1978) Corneal topography and monocular diplopia following near work. *Am. J. Optom. Phys. Opt.* **55,** 818–823.

Campbell, C. (1998) Corneal aberrations, monocular diplopia, and ghost images: analysis using corneal topographical data. *Optom. Vis. Sci.* **75,** 197–207.

Carney, L. G., Liubinas, J. and Bowman, K. J. (1981) The role of corneal distortion in the occurrence of monocular diplopia. *Acta Ophthalmol.* **59,** 271–274.

Cheng, X., Bradley, A., Hong, X. and Thibos, L. N. (2003) Relationship between refractive error and monochromatic aberrations of the eye. *Optom. Vis. Sci.* **80,** 43–49.

Coffeen, P. and Guyton, D. L. (1988) Monocular diplopia accompanying ordinary refractive errors. *Am. J. Ophthalmol.* **105,** 451–459.

Fincham, E. F. (1963) Monocular diplopia. *Br. J. Ophthalmol.* **7,** 705–712.

Ford, J. G., Davis, R. M., Reed, J. W., Weaver, R. G., Craven, T. W. and Tyler, M. E. (1997) Bilateral monocular diplopia associated with lid position during near work. *Cornea* **16,** 525–530.

Fujikado, T., Kuroda, T., Maeda, N., Kim, A., Tano, Y., Oshika, T., Hirohara, Y. and Mihashi, T. (2004) Wavefront analysis of monocular triplopia in the eye of nuclear cataract. *Am. J. Ophthalmol.* **137,** 361–363.

Golnik, K. C. and Eggenberger, E. (2001) Symptomatic corneal topographic change induced by reading in down gaze. *J. Neuro-ophthalmol.* **21,** 199–204.

Goss, D. A. and Criswell, M. H. (1992a) Bilateral monocular diplopia following television viewing. *Clin. Eye Vis. Care* **52,** 139–140.

Goss, D. A., West, R. W., Carr, L. W. and Edmondson, L. L. (1992b) A case of monocular triplopia of lenticular origin. *Optom. Vis. Sci.* **69,** 486–488.

Kaufman, B. H. and Sugar, J. (1996) Discrete nuclear sclerosis in young patients with myopia. *Arch. Ophthalmol.* **114,** 1178–1180.

Kluxen, G. (1985) Die polyopia monocularis bei kernkataract. *Klin. Mbl. Augenheilkd.* **187,** 270–272.

Kommerell, G. (1993) Monocular diplopia caused by pressure of the upper eyelid on the cornea. Diagnosis based on the "Venetian blind phenomenon" in streak retinoscopy. *Klin. Monatsbl. Augenheilkd.* **203,** 384–389.

Kuroda, T., Fujikado, T., Maeda, N., Oshika, T., Hirohara, Y. and Mihashi, T. (2002a) Wavefront analysis of higher order aberrations in patients with cataracts. *J. Cat. Ref. Surg.* **28,** 438–444.

Kuroda, T., Fujikado, T., Ninomiya, S., Maeda, N., Hirohara, Y. and Mihashi, T. (2002b) Effect of aging on ocular light scatter and higher order aberrations. *J. Refract. Surg.* **18,** S598–S602.

Kuroda, T., Fujikado, T., Maeda, N., Oshika, T., Hirohara, Y. and Mihashi, T. (2002c) Wavefront analysis in eyes with nuclear or cortical cataract. *Am. J. Ophthalmol.* **134,** 1–9.

Kuszak, J. R., Peterson, K. L., Sivak, J. G. and Herbert, K. L. (1994) The interrelationship of lens anatomy and optical quality II. Primates Lenses. *Exp. Eye Res.* **59,** 521–535.

Lee, A. G. and Brazis, P. W. (2003) *Clinical Pathways in Neuro-ophthalmology*, 2nd edn. Thieme, NY, pp. 215–217.

Mandell, R. B. (1996) Bilateral monocular diplopia following near work. *Am. J. Optom. Arch. Am. Acad. Optom.* **43,** 500–504.

Trobe, J. D. (2001) *The Neurology of Vision.* Oxford University Press, Oxford, pp. 77–79.

Woods, R. L., Bradley, A. and Atchison, D. A. (1996a) Monocular diplopia caused by ocular aberrations and hyperopic defocus. *Vis. Res.* **36,** 3597–3606.

Woods, R. L., Bradley, A. and Atchison, D. A. (1996b) Consequence of monocular diplopia for contrast sensitivity function. *Vis. Res.* **36,** 3587–3596.

after systemic therapy. The patient denied any contact with cats, and similar cases without exposure to cats have been reported.[3]

Unilateral elevation of IOP could be coincidental. However, the lack of a family history of glaucoma or other signs of unilateral glaucoma (keratic precipitates, heterochromia, rubeosis, pigment dispersion, pseudoexfoliation, plateau iris configuration, trabeculodysgenesis, or ultrasonic signs of ciliochoroidal detachment or swelling/anteroversion of the ciliary body) ruled out other possible associations and led to the reasonable assumption of a causal connection.

IOP elevation in inflammatory diseases of the eye is a well-known phenomenon. Possible causative mechanisms in uveitis-induced open-angle glaucoma are obstruction of the trabecular meshwork by precipitates, cellular debris, or serum proteins. In addition, secretion of prostaglandins can cause an increase of vascular permeability and swelling of the trabeculum itself (trabeculitis). Loss of or damage to the trabecular endothelial cells can lead to an increase in the outflow resistance, and a breakdown of the blood-aqueous barrier can cause elevation of the aqueous viscosity. Thus, the mild morphological changes occurring as the IOP rose in no way contradict a possible causal connection between inflammation and blocking of the outflow facility. The anterior synechiae later seen in our patient suggest that the anterior segment had also been a target of the inflammation.

Ocular CSD should be included in the differential diagnosis of unilateral secondary glaucoma. Diagnosis can be made by serological evidence or direct DNA analysis of ocular fluids.[4] Currently, the necessity of antibiotic treatment of ocular CSD is controversial because of its self-limiting character.[5] Some clinicians recommend only observation and patient education owing to the absence of controlled clinical trials and possible side effects of the antibiotic medication. Nevertheless, significant long-term sequelae are not very common and most previous reviews have shown not only good visual recovery but also that oral antibiotic medications are well tolerated and lead to prompt improvement of systemic and ocular symptoms.[1,3] Additionally, a few cases with severe vision loss or involvement of the central nervous system indicate the possible benefit of early therapy.

This case of CSD with concomitant glaucoma underlines the importance of regular IOP measurements in such cases, despite the absence of marked anterior involvement.

**Key Words:** *Bartonella henselae*, cat-scratch disease, neuroretinitis, secondary glaucoma

Focke Ziemssen, Karl-Ulrich Bartz-Schmidt, and Faik Gelisken
University Eye Hospital Department I, Tuebingen, Germany

Received: October 23, 2004 / Accepted: June 13, 2005
Correspondence to: Focke Ziemssen, University Eye Hospital Tuebingen, Schleichstr. 12, 72076 Tuebingen, Germany
e-mail: Focke.Ziemssen@med.uni-tuebingen.de

DOI 10.1007/s10384-005-0278-9

## References

1. Cunningham ET, Koehler J. Ocular bartonellosis. Am J Ophthalmol 2000;130:340–349.
2. Suhler EB, Lauer AK, Rosenbaum JT. Prevalence of serologic evidence of cat-scratch disease in patients with neuroretinis. Ophthalmology 2000;107:871–876.
3. Ormerod LD, Dailey JP. Ocular manifestations of cat-scratch disease. Curr Opin Ophthalmol 1999;10:209–216.
4. Labalette P, Bermond D, Dedes V, Savage C. Cat-scratch disease neuroretinitis diagnosed by a polymerase chain reaction approach. Am J Ophthalmol 2001;132:575–576.
5. Rosen B. Management of *B. henselae* neuroretinitis in cat-scratch disease. Ophthalmology 1999;106:1–2.

# Null *ABCA4* Gene Mutations Found in Japanese Patients with Panretinal Degeneration

Although typical Stargardt disease (STGD), autosomal recessive cone–rod dystrophy (CRD), and autosomal recessive retinitis pigmentosa (RP) have several different criteria of diagnosis, retina-specific ATP-binding cassette transporter (*ABCA4*) gene mutations are responsible for some cases of CRD and RP, as well as for STGD.[1–5] Upon fluorescein angiography (FA), STGD patients have diagnostic yellow-white fundus flecks and a "dark choroid".

CRD and RP patients are distinguished according to which type of photoreceptor is mainly affected. In this report, we describe two patients with pigmented panretinal degeneration who carry allelic null mutations in the *ABCA4* gene.

## Case Reports

Patient F104-IV-1 (male) presented with initial complaints of decreased central vision at 7 years of age and became conscious of night blindness in his third decade of life. During his childhood, he had been found at another hospital to be suffering from macular degeneration, and he exhibited progressive central scotoma. When he was first examined at our hospital, at 26 years of age, his visual acuities were severely decreased (20/2000 in the right eye and 20/1000 in the left eye) with only peripheral visual fields remaining. Funduscopy disclosed pigmented retinal degeneration (Fig. 1, top left). He was found to have an almost complete loss of both photopic and scotopic functions. FA showed chorioretinal degeneration extending to the vascular arcade (Fig. 1, bottom left). He was found by sequence analysis to be homozygous for the Arg2149stop mutation of the *ABCA4* gene (Fig. 2).

Patient F128-II-2 (male) presented with initial complaints of decreased central vision at 7 years of age and was conscious of night blindness from an early stage of the disease. During his childhood, he also was found, at another

Jpn J Ophthalmol
Vol 50: 176–190, 2006

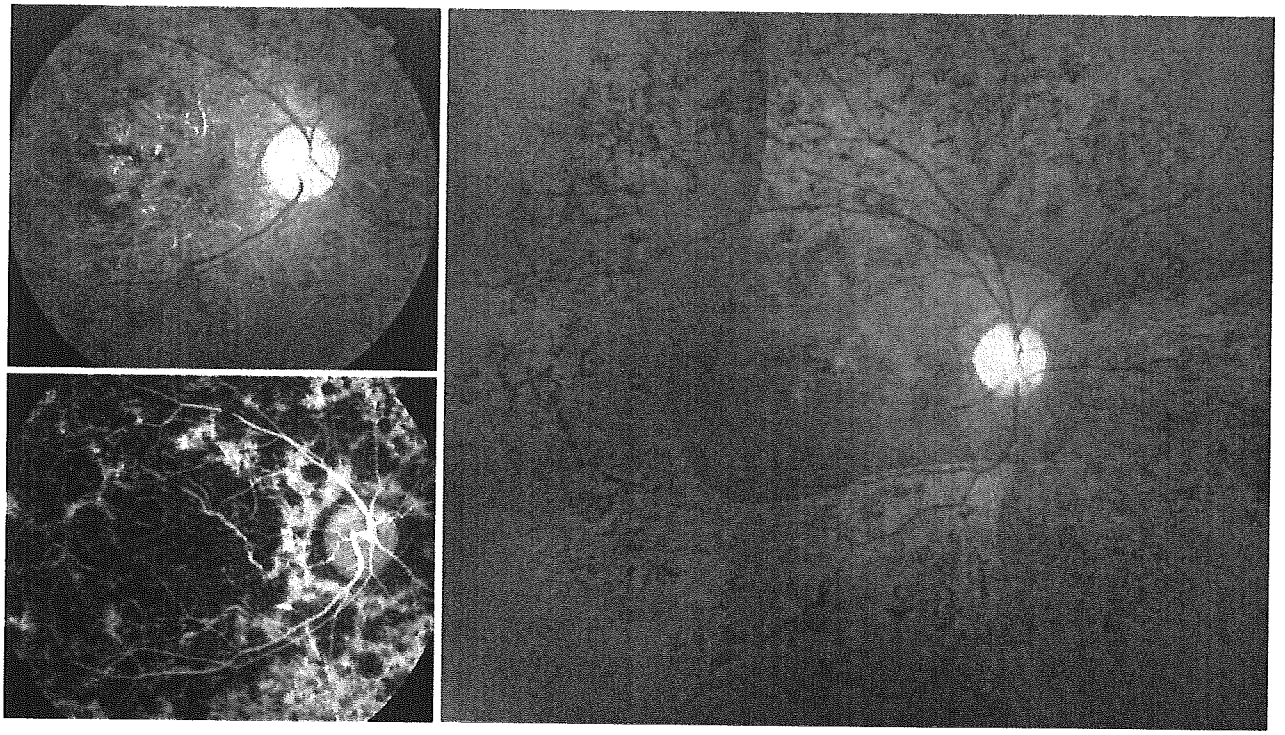

**Figure 1.** (*Top left*) and (*right*) Fundus photographs of patients F104-IV-1 and F128-II-2, repectively, showing severe retinal pigment epithelium degeneration, bone spicule-like pigmentation, and slightly attenuated retinal vessels extending to the midperiphery. (*Bottom left*) Fluorescein angiography of patient F104-IV-1 showing chorioretinal degeneration extending to the vascular arcade.

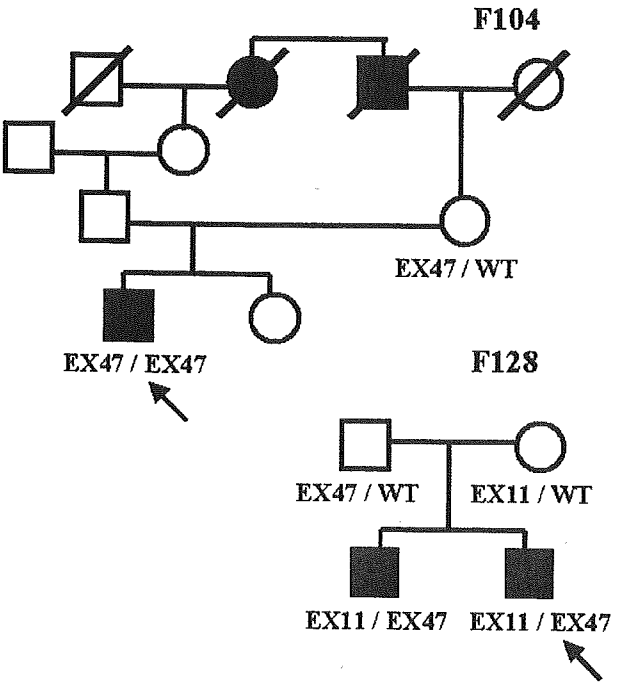


**Figure 2.** Two mutations completely segregated with the disease. *WT*, wild type; *EX11*, Lys461stop; *EX47*, Arg2149stop.

hospital, to be suffering from macular degeneration, and he exhibited progressive central scotoma. When he was first examined in our hospital, at 25 years of age, his visual acuities were severely decreased (finger count in the right eye and 20/2000 in the left eye). The fundus appearance was very similar to that of patient F104-IV-1, with only peripheral visual fields remaining and almost complete loss of both photopic and scotopic functions (Fig. 1, right). We could not perform FA. Patient F128-II-1 showed a similar clinical course. He was found to be compound heterozygous for the Lys461stop and Arg2149stop mutations by sequence analysis (Fig. 2).

## Comments

A novel null mutation (Lys461stop) and a known null mutation (Arg2149stop) were identified in these two patients by sequence analysis. Patient F104-IV-1 was found to be homozygous for the Arg2149stop mutation, and patient F128-II-2 was found to be compound heterozygous for the Lys461stop and Arg2149stop mutations (Fig. 2). We diagnosed both patients as having central RP, but we could not completely distinguish between CRD and RP in these patients, because early electroretinogram (ERG) recordings were not available. The ERG recorded at our hospital

represented the final stage of the disease, with absence of both cone and rod responses. According to a genotype–phenotype analysis of the *ABCA4* gene, there is an inverse relationship between the presumed residual ABCA4 function and the severity of the disorder, and the *ABCA4* gene mutations associated with CRD and RP are similar in this respect.[3,4] These two cases are consistent with this previous genotype–phenotype analysis. Furthermore, we previously reported that RP resulting from *ABCA4* null mutations can exhibit the clinical phenotypes of STGD in the early course of the disease.[5] During childhood, the two patients in this report had been found at another hospital to be suffering from macular degeneration. Although neither ERG nor FA findings were available for the early stage of the disease in either patient, we were able to identify the pathogenesis of these patients by sequence analysis. Therefore, sequence analysis is useful for the diagnosis of panretinal degeneration.

**Key Words:** *ABCA4* gene, cone–rod dystrophy, retinitis pigmentosa, Stargardt disease

Takehiro Fukui, Takashi Fujikado, Motokazu Tsujikawa, Masaki Okada, Shuji Yamamoto, and Yasuo Tano
Department of Ophthalmology, Osaka University Graduate School of Medicine, Osaka, Japan

Received: April 2, 2004 / Accepted: May 27, 2005
Correspondence to: Takashi Fujikado, Department of Ophthalmology, Osaka University Graduate School of Medicine, 2-2 Yamadaoka, Suita, Osaka 565-0871, Japan
e-mail: fujikado@ophthal.med.osaka-u.ac.jp

DOI 10.1007/s10384-005-0279-8

## References

1. Allikmets R, Singh N, Sun H, et al. A photoreceptor cell-specific ATP-binding transporter gene (*ABCR*) is mutated in recessive Stargardt macular dystrophy. Nat Genet 1997;15:236–246.
2. Martinez-Mir A, Paloma E, Allikmets R, et al. Retinitis pigmentosa caused by a homozygous mutation in the Stargardt disease gene *ABCR*. Nat Genet 1998;18:11–12.
3. Maugeri A, van Driel M, van de Pol DR, et al. The 2588G→C mutation in the *ABCR* gene is a mild frequent founder mutation in the Western European population and allows the classification of *ABCR* mutations in patients with Stargardt disease. Am J Hum Genet 1999;64:1024–1035.
4. Briggs CE, Rucinski D, Rosenfeld PJ, Hirose T, Berson EL, Dryja TP. Mutations in *ABCR* (*ABCA4*) in patients with Stargardt macular degeneration or cone–rod degeneration. Invest Ophthalmol Vis Sci 2001;42:2229–2236.
5. Fukui T, Yamamoto S, Nakano K, et al. *ABCA4* gene mutations in Japanese patients with Stargardt disease and retinitis pigmentosa. Invest Ophthalmol Vis Sci 2002;43:2819–2824.

# A Case of Idiopathic Retinal Vasculitis, Aneurysm, and Neuroretinitis Effectively Treated by Steroid Pulse Therapy

Idiopathic retinal vasculitis, aneurysm, and neuritis (IRVAN) is a relatively rare syndrome clinically characterized by peripheral retinal vascular occlusion and idiopathic posterior retinal vasculitis associated with multiple posterior retinal artery aneurysms.[1] In terms of visual prognosis of this syndrome, relatively well-preserved visual acuities have been reported in most cases, but some cases with poor outcomes have also been recognized.[1] Although several therapies, including oral corticosteroid administration,[1–5] laser photocoagulation,[1,4,5] and surgical intervention[1,5] have been utilized, the effectiveness of these therapies is uncertain. Here, we present the case of a young boy with IRVAN, who initially showed progressive deterioration of visual acuity despite photocoagulation toward the midperipheral venous occlusion and oral corticosteroid administration, but who thereafter improved remarkably with steroid pulse therapy.

## Case Report

A 15-year-old boy who presented with a sudden onset of visual deterioration in his right eye was referred to Oodate City Hospital. Best-corrected visual acuity was 20/40 OD and 20/20 OS. Funduscopy examination and fluorescein angiography (Fig. 1A) revealed bilateral swollen discs, temporal peripapillary exudates, posterior retinal vasculitis with multiple aneurysms (Fig. 1B, top), and midperipheral venous occlusion. No abnormal results were obtained from laboratory tests, which included urinalysis, complete blood cell count, erythrocyte sedimentation rate, immunoglobulin electrophoresis, blood chemistry, serum angiotensin-converting enzyme, rheumatoid factor, anti-*Bartonella* antibodies, anticardiolipin, lupus anticoagulant, antinuclear antibody, serum antibodies to viruses, cerebrospinal fluid, chest X-ray, and head magnetic resonance imaging. On the basis of these findings, the patient was diagnosed as having IRVAN. He was then treated with oral prednisolone (30 mg/day) for retinal vasculitis and laser photocoagulation (Nidek ADC-8000 610-nm dye laser; Nidek, Gamagori, Aiichi, Japan; spot size, 300 μm; exposure time, 0.2 s; power, 0.18–0.2 mW) for midperipheral retinal vascular occlusion (Fig. 1B, bottom) extended to all four quadrants of his right eye (total, 1307 shots) and to the upper and lower nasal quadrants of his left eye (total, 739 shots). However, despite these therapies, his best-corrected visual acuity worsened to 20/200 OD and 20/40 OS. Moreover, peripapillary subretinal fluid and temporal peripapillary subretinal lipid exudates became more extensive, and optic nerve swelling became more remarkable. He was then referred to Hirosaki

# Long-term Results of Vitrectomy without Laser Treatment for Macular Detachment Associated with an Optic Disc Pit

*Akito Hirakata, MD, Annabelle A. Okada, MD, Tetsuo Hida, MD*

***Purpose:*** To evaluate the efficacy of vitrectomy and gas tamponade, without laser photocoagulation to the margin of the optic nerve, for the treatment of macular detachment associated with an optic disc pit.

***Design:*** Noncomparative interventional case series.

***Participants:*** Eleven consecutive patients (8–47 years of age) who presented with unilateral macular detachment associated with an optic disc pit.

***Intervention:*** Pars plana vitrectomy, induction of posterior vitreous detachment (PVD), and gas tamponade were performed, with postoperative facedown positioning for 1 week. The presence of a double-layer detachment consisting of an inner layer separation and an outer layer detachment was observed in 10 of 11 eyes either preoperatively or postoperatively. Patients were observed for 10 to 98 months (mean, 47) after surgery.

***Main Outcome Measures:*** Anatomic outcome and visual acuity were retrospectively analyzed for all eyes. Optical coherence tomography was used to observe anatomic changes in the macula in some eyes.

***Results:*** Complete retinal reattachment was achieved in 10 of 11 eyes, although these eyes required nearly 1 year to reach this state. The one eye with persistent retinal detachment was observed to have a marked reduction of the detachment by 10 months postoperatively. No recurrences were observed. Visual acuity improvement was documented in 7 of 11 eyes.

***Conclusions:*** These results suggest that vitrectomy with induction of PVD and gas tamponade, without additional laser treatment, is successful in reattaching the macula and improving central vision in most patients with optic disc pit maculopathy. *Ophthalmology 2005;112:1430–1435 © 2005 by the American Academy of Ophthalmology.*

Congenital pit of the optic nerve head is a rare anomaly first described by Wiethe in 1882.[1] Approximately two thirds of patients have a concurrent or previous associated serous retinal detachment (RD) of the macula.[2–4] The age at onset of the RD is variable, with the mean being 30 years. The pathogenesis of optic disc pit maculopathy is unknown. In 1988, based on a study of stereoscopic transparencies and visual fields (VFs), Lincoff et al proposed that fluid from the optic disc pit creates a schisislike inner layer separation of the retina.[5] The outer layer detachment centered over the macula was suggested to be a secondary phenomenon. More recently, several authors have confirmed the 2-layer structure of optic disc pit maculopathy using optical coherence tomography (OCT).[6–8]

The treatment of serous RD associated with an optic disc pit is still controversial. The use of laser therapy to produce a barrier of chorioretinal adhesions at the optic disc border is often unsuccessful, and repeated treatments are needed.[9–11] Several reports suggest that vitrectomy combined with laser photocoagulation and gas tamponade may be more effective than external laser therapy alone, particularly in eyes with severe visual loss.[12–15] Theodossiadis reported that macular scleral buckling can yield favorable anatomical and functional results.[16] Lincoff et al reported that intravitreal gas injection alone can induce pneumatic displacement of the outer layer detachment and improve central vision.[17] However, the effect may only be temporary, because recurrence caused by fluid movement from the remaining inner layer separation was found by OCT.[8]

Bonnet reported that none of 25 eyes with macular detachment associated with optic disc pit had a posterior vitreous detachment (PVD), and that 2 of the eyes had spontaneous reattachment of the macula after development of PVD.[18] Gordon and Chatfield[19] and Gass[10] found no evidence of PVD in their cases, and suggested that vitreous traction on the macula may cause passive migration of fluid into the submacular space via the pit. Recent experience with the surgical treatment of macular holes and macular edema has shown the importance of vitreous tangential traction in thepathogenesis of these diseases.[20–22] Similar tangential vitreous traction at the pit, an area of abnormal

Originally received: September 27, 2004.
Accepted: February 5, 2005. Manuscript no. 2004-139.

From Kyorin Eye Center, Kyorin University School of Medicine, Tokyo, Japan.

Presented in part at: American Academy of Ophthalmology Annual Meeting, October, 1996; Chicago, Illinois.

Correspondence and reprint requests to Akito Hirakata, MD, Department of Ophthalmology, Kyorin University School of Medicine, 6-20-2 Shinkawa, Mitaka, Tokyo 181-8611 Japan. E-mail: hirakata@eye-center.org.



ISSN 0161-6420/05/$–see front matter
doi:10.1016/j.ophtha.2005.02.013

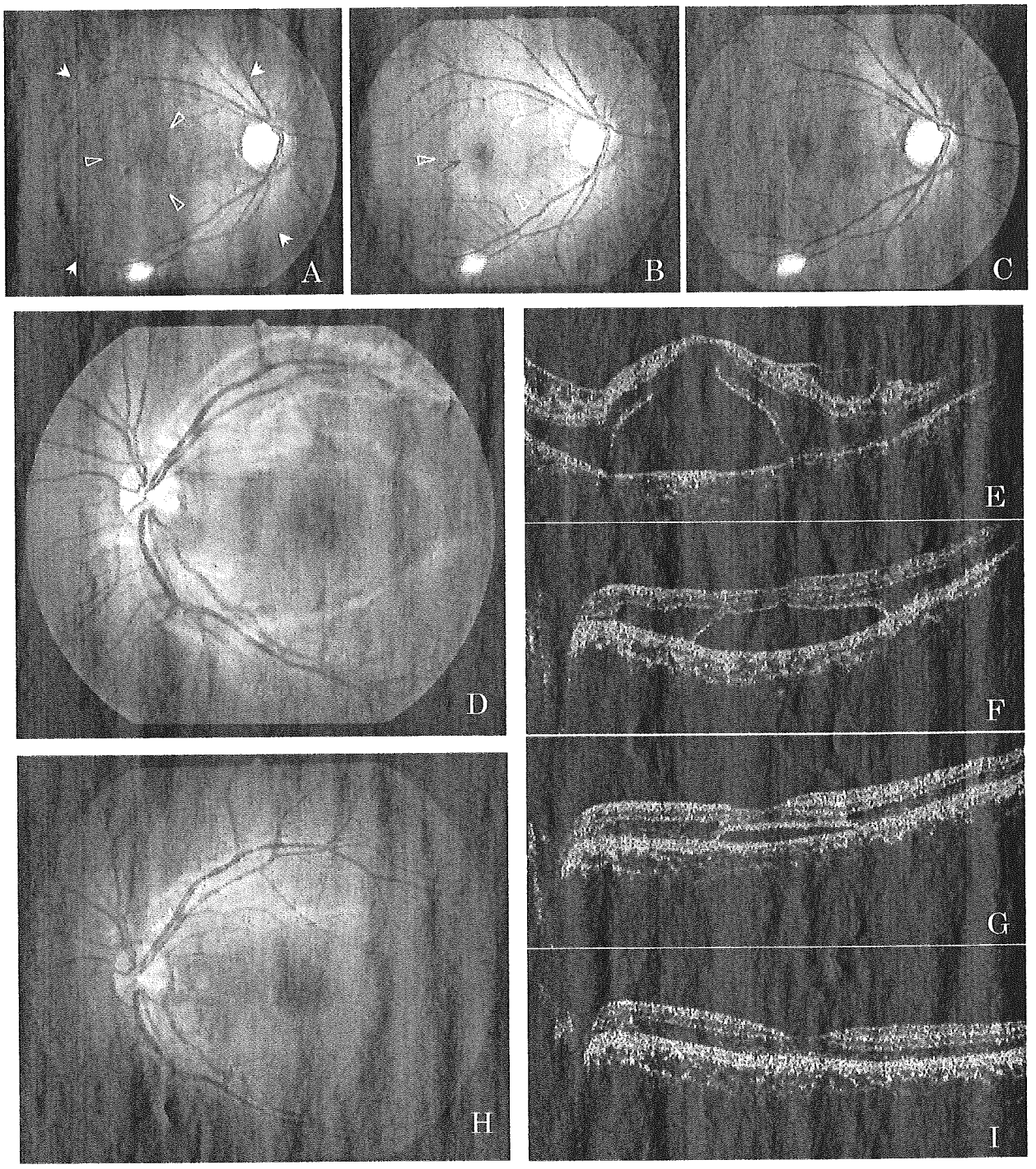


**Figure 1.** Composite of representative clinical findings from patients 1 (**A–C**) and 10 (**D–I**). All optical coherence tomography (OCT) scan lengths were 10 mm. **A**, Photograph of patient 1's right fundus preoperatively, showing an inferotemporal optic disc pit associated with a large oval-shaped area of macular detachment (large arrows), a nerve fiber layer defect leading from the optic disc pit (green arrow), and an area of myelinated nerve fibers in the inferior macula. The outer layer hole (blue arrow) and the round 1.5–disc diameter outer layer detachment (white open arrowheads) also shown were not present initially but developed after 4 months of follow-up. Preoperatively, the best-corrected visual acuity (VA) was 0.2. **B**, Two months after vitrectomy and gas tamponade, an irregularly shaped break was noted in the outer layer (blue arrow), with the outer layer detachment (white open arrowheads) being slightly enlarged. A new nerve fiber layer defect was also observed leading from the superotemporal edge of the optic disc (green arrows). **C**, One year postoperatively, the macula was observed to be completely reattached, with a VA of 1.0. The nerve fiber layer defects remained unchanged. **D**, Fundus photograph of patient 10's left eye at presentation, showing a shallow retinal elevation extending from the superotemporal to inferotemporal arcades. A round 2–disc diameter outer layer detachment was also observed in the center of the macula, and preoperatively, VA was 0.08. **E**, Optical coherence tomography at presentation revealed an inner layer separation as well as a hole in the outer layer detachment at the macula and an outer layer detachment surrounding the hole. **F**, Three months after vitrectomy and gas tamponade, OCT showed a decrease in the inner layer separation and outer layer detachment. **G**, At 9 months, OCT showed resolution of the inner layer separation but a residual outer layer detachment. **H, I**, Fundus photograph and OCT at 12 months postoperatively showing the macula completely reattached and the optic disc pit appearing grayer and deeper than preoperatively. Visual acuity was 1.2.

Table 1. Clinical

| Patient | Age (yrs) | Gender | Eye | Refractive Error (Diopters) | Symptom | Preoperative Best-Corrected Visual Acuity | Pit Location |
|---|---|---|---|---|---|---|---|
| 1 | 40 | F | R | −2.0 | Central scotoma | 0.3 | Inferotemporal |
| 2 | 15 | F | L | −1.0 | Decreased VA | 0.2 | Inferotemporal |
| 3 | 43 | F | L | −1.5 | Central scotoma | 0.08 | Temporal |
| 4 | 30 | M | R | −0.5 | Central scotoma | 0.6 | Temporal |
| 5 | 22 | M | L | −1.0 | Metamorphopsia | 0.5 | Inside in coloboma |
| 6 | 19 | M | R | 0.0 | Central scotoma | 0.4 | Temporal |
| 7 | 24 | M | L | 0.0 | Central scotoma | 0.6 | Inferior |
| 8 | 42 | F | R | −1.0 | Metamorphopsia | 1.0 | Central |
| 9 | 47 | M | L | 0.0 | Central scotoma | 0.2 | Inferotemporal |
| 10 | 8 | F | L | −1.0 | Decreased VA | 0.08 | Temporal |
| 11 | 44 | F | R | 0.0 | Decreased VA | 0.4 | Temporal |

F = female; L = left; M = male; R = right; VA = best-corrected visual acuity; VF = visual field.
+, present; −, absent.
*Duration in months.
†Displacement of subretinal fluid immediately after surgery.

configuration of the optic disc, may cause migration of fluid into intraretinal spaces. We believe that posterior vitreous traction on the margin of the optic disc pit may play an important role in the pathogenesis of this disease. There have been several reports regarding the efficacy of vitrectomy and gas tamponade with conflicting results, some reporting the recurrence of macular detachment with long-term follow-up after surgery.[8,12–14] However, most of these reports did not specify whether PVD induction was performed, and some stated that only core vitrectomy permitting space for a 60% to 70% gas tamponade was performed.

The purpose of this study was to examine long-term clinical outcomes in 11 eyes that underwent vitrectomy with PVD induction and gas tamponade, without laser application, for the treatment of optic disc pit maculopathy.

## Patients and Methods

Eleven eyes of 11 consecutive patients who presented to the Kyorin Eye Center with an optic disc pit associated with macular detachment were included in this study. Institutional review board approval was not required, and records were reviewed retrospectively. Best-corrected visual acuity (VA) was recorded, and indirect funduscopy, slit-lamp biomicroscopy using a contact lens, and Goldman VF examinations were performed preoperatively and postoperatively. Scanning laser ophthalmoscopy and fluorescein angiography were done preoperatively to confirm the optic disc pit and macular abnormalities in some patients. Optical coherence tomography (Zeiss-Humphrey, San Leandro, CA) was used to observe posterior retinal changes in cases with follow-up from 1999 on.

Surgery was performed for the indication of worsening VA or for macular detachment persisting for ≥3 months. All surgeries were performed by the same surgeon (AH) between July 1994 and October 2003, and patients were observed postoperatively for 10 to 98 months (mean, 47). Vitrectomy was performed with the intention of releasing vitreous traction at the optic disc pit. Posterior vitreous detachment was initiated by suction over the optic disc or near areas of retinal schisis using the vitreous cutter. To limit retinal damage secondary to surgical manipulation, special attention was given to separating the posterior hyaloid gently over schisis areas. Triamcinolone acetonide[23,24] was used intraoperatively in 2 eyes (patients 10 and 11) and fluorescein dye[25,26] in 1 eye (patient 2) to highlight the posterior hyaloid membrane. After removal of the posterior hyaloid over the posterior pole, fluid–air exchange was performed, followed by gas tamponade with either 15% to 20% sulfur hexafluoride or 14% perfluoropropane and postoperative facedown positioning for approximately 1 week.

Cataract surgery was not performed, except in patient 3, who underwent lens extraction and intraocular lens implantation during a second vitrectomy procedure to close a macular hole.

## Results

### Clinical Characteristics

The clinical characteristics of all 11 patients are shown in Table 1, and clinical photographs of representative patients are shown in Figure 1. Six of the patients were women and 5 were men, with ages ranging from 8 to 47 years (mean, 30.4). All patients were of Japanese ethnicity, except for patient 7, who was Caucasian. All patients complained of a central scotoma or metamorphopsia in the affected eye for several months. None of the affected eyes had severe refractive errors, and preoperative VA ranged from 0.08 to 1.0 (mean, 0.3). Patient 7 had received previous treatment for the optic disc pit maculopathy, consisting of laser photocoagulation to the edge of the optic disc pit, but no other patients had received any prior treatment. Nine of the 11 patients had no pertinent medical or ocular history. Patient 10 was referred to our hospital for visual disturbance after blunt ocular trauma by a volleyball, at which time macular detachment associated with an optic disc pit was diagnosed in the injured eye. Patient 8 had a history of RD surgery in the fellow eye.

The presence of a double-layer detachment, consisting of both an inner layer separation and an outer layer detachment, was confirmed either before or after surgery in 10 of 11 eyes. The outer layer detachment did not seem to communicate with the optic disc in 8 eyes, but did seem to do so in 2 eyes. An irregularly shaped outer layer break and outer layer detachment were observed to develop after schisislike inner layer separation in patients 1 (Fig 1A) and 4 preoperatively and in patient 8 postoperatively. An outer layer break in the macula was present or developed sometime

Characteristics

| Duration of Symptom* | Double Layer Retinal Detachment | Outer Layer Hole at Fovea | Posterior Vitreous Detachment | Duration until Macular Attachment* | Final Best-Corrected Visual Acuity | Complications | Follow-up* |
|---|---|---|---|---|---|---|---|
| 5.0 | + | + | − | 12 | 1.2 | Peripheral VF defect | 80 |
| >36.0 | + | + | − | 2 | 0.04 | Retinal damage | 91 |
| 6.0 | + | + | − | 5 | 0.1 | — | 98 |
| 6.0 | + | + | − | 8 | 0.8 | Retinal break | 24 |
| 2.0 | − | − | − | 12† | 1.2 | — | 73 |
| 9.0 | + | + | − | 12† | 1.0 | — | 37 |
| 24.0 | + | − | − | 12† | 1.2 | — | 15 |
| 2.0 | + | + | − | 15 | 1.0 | — | 57 |
| 3.0 | + | + | − | 10 | 1.2 | — | 14 |
| 5.0 | + | + | − | 12 | 1.2 | — | 12 |
| 24.0 | + | + | − | Flatter | 1.0 | — | 10 |

during the clinical course in a total of 9 of the 11 eyes. One eye (patient 3) had a full-thickness macular hole preoperatively. Neither PVD nor vitreomacular or vitreopapillary traction was observed in any eyes preoperatively by fundus biomicroscopy; OCT performed preoperatively in 5 eyes also did not reveal vitreomacular or vitreopapillary traction.

## Anatomic Results

Complete retinal reattachment was achieved in 10 of 11 eyes, although these eyes required nearly 1 year to reach this state (Fig 1). Interestingly, after surgery the outer layer break seemed to enlarge temporarily in most cases (Fig 1B). One eye had persistent RD after surgery, but was documented by OCT to have marked reduction of the detachment by 10 months postoperatively. No recurrences were observed in any eyes.

Observation by OCT showed slow absorption of the inner layer separation and outer layer detachment after surgery, with complete absorption of fluid after 2 to 15 months (Fig 1E–G, I). The macular hole present preoperatively in patient 3 remained open after surgery, but without surrounding RD (fluid cuff) or retinal edema. However, 3 years postoperatively a fluid cuff appeared around the macular hole, with corresponding decrease in vision, and a second vitrectomy procedure with internal limiting membrane peeling and gas tamponade successfully closed the hole.

Two patients (5 and 11) also had an optic disc coloboma, with the optic disc pit present within the area of the coloboma. The pits were not obvious preoperatively; however, postoperatively, as the retina reattached, the pits were easily observed as being darker and deeper relative to the surrounding colobomatous areas.

## Visual Acuity Results

Preoperative and final VAs are shown in Table 1. Despite evidence of residual shallow inner layer separation and outer layer detachment, VA started to improve within a few months in most eyes. Improvement in VA of 0.2 logarithms of the minimum angle of resolution or greater was documented in 7 of 11 eyes. Nine of 11 eyes had a postoperative VA of 0.8 or better.

## Complications

Intraoperative or postoperative complications were observed in 3 patients. Patient 1 developed a dense scotoma in the inferotemporal quadrant with a nerve fiber layer defect between 12-o'clock and 3-o'clock at 2 weeks postoperatively (Fig 1B). At final examination 1 year postoperatively, VA was 1.0, with the macula reattached and no change in the nerve fiber layer defect (Fig 1C).

Patient 2, a 15-year-old girl, underwent vitrectomy and fluorescein dye–assisted PVD induction followed by 15% sulfur hexafluoride tamponade. The surgeon noted difficulty in inducing the PVD, resorting to the use of a retinal pick and forceps in addition to cutter suction. A few drops of 2% fluorescein dye were introduced to the infusion line to highlight the posterior hyaloid membrane.[25,26] A tiny hemorrhage was noted at the superior margin of the optic disc after complete vitreous separation. On the second postoperative day, the patient complained of darkened vision, and whitening of the retina was observed around the optic disc in a gas-filled eye. Fluorescein angiography showed normal arm-to-retina circulation times. Oral prednisolone at a dose of 40 mg tapered to 30 mg was administered for a total of 9 days for the possibility of inflammation related to the surgical manipulation or phototoxicity, but the retinal findings remained unchanged. Electoretinography performed on the fifth postoperative day showed a negative b-wave and a reduced a-wave. Pigmented atrophy of the peripapillary area developed over 6 months.

Patient 4 developed an iatrogenic peripheral retinal break intraoperatively during PVD induction that was treated successfully with laser photocoagulation.

# Discussion

In this study, we were able to confirm Lincoff et al's notion of a double-layer detachment in 10 of 11 eyes with optic disc pit maculopathy.[5] An outer layer detachment was observed either preoperatively or postoperatively as a secondary phenomenon, developing after presence of an inner layer separation in 3 eyes. In the remaining 7 eyes, the outer layer detachment, along with an outer layer break, was observed at presentation.

Lincoff et al reported on the successful use of intravitreal gas tamponade without vitrectomy to induce pneumatic displacement of the outer layer detachment and improve central vision.[17] However, OCT findings have suggested that fluid may continue to flow from the remaining inner layer separation to the outer layer detachment.[8] Because we

believe that vitreoretinal traction is an important factor in the pathogenesis of macular detachment associated with an optic disc pit, we feel that vitrectomy with complete PVD induction is essential for the treatment of these eyes. We postulate that vitreous traction may play a critical role in the development of these detachments, although we were unable to detect any vitreomacular or vitreopapillary traction by OCT. The added use of gas tamponade probably helps to push fluid from the inner layer separation into the outer layer detachment. Because we did not apply laser photocoagulation at the optic disc pit margin in our patients, we deduce that release of continued vitreoretinal traction by surgical induction of PVD was sufficient to lead to diminishment of new fluid accumulation in the inner layer separation presumably coming from the optic disc pit. This idea is supported by our postoperative OCT findings in patient 10, showing that the inner layer separation resolved first, before resolution of the outer layer detachment.

Vitrectomy with gas tamponade, with or without laser application to the margin of the pit, for macular detachment associated with an optic disc pit has been reported.[12–14] However, these series did not achieve VA results as good as those of the current study, and had higher rates of reoperation. This difference may be due to differences in surgical technique. Furthermore, the current study did not employ any laser application to achieve good visual and anatomical outcomes, and we believe that assuring a complete PVD induction during surgery played an integral part in achieving these results.

Favorable visual and anatomical outcomes have also been reported using macular buckling in Theodossiadis's series of 9 consecutive patients with optic disc pit maculopathy.[16] Recently, Theodossiadis and Theodossiadis have also reported on OCT findings in 26 eyes treated with scleral buckling, with resolution of macular detachment noted in 24 eyes. Disappearance of intraretinal fluid over 7 to 9 months postoperatively was documented in 4 of 5 eyes that were evaluated by OCT both before and after surgery.[27] We believe that these favorable results with scleral buckling are due to conversion of the inward perpendicular component of the vector, caused by tangential forces associated with posterior hyaloid traction on the retina at the irregular surface of the optic disc, to an outward perpendicular vector component by the scleral buckle promoting attachment of the retina.[28]

Spontaneous resolution of the macular detachment associated with optic nerve pits is also known to occur in approximately 25% of untreated patients.[4] However, cystic retinal degeneration, macular hole formation, and retinal pigment epithelial atrophy often limit visual recovery in these cases. Over half of eyes with macular detachments experience a decrease in VA to 20/100 or less within 5 years.[3] In contrast, although the time to best VA took close to 6 months in most patients, 9 of 11 eyes eventually achieved a postoperative VA of 0.8 or greater. Furthermore, we found that VA started to improve after surgery despite the continued, albeit decreased, presence of inner layer separation and outer layer detachment in the fovea by OCT. This suggests that mild improvements in foveal contour alone may lead to improved vision and that long-term observation is essential postoperatively in these eyes. In eyes that have undergone vitrectomy, additional treatments for the macular detachment should not be contemplated too early. Furthermore, given the fact that subretinal fluid persisted for a long time postoperatively but eventually resolved, gas tamponade may actually not be necessary for successful treatment. Because all eyes in the current study received gas tamponade, we are not able to assess this possibility.

Complications associated with surgery included VF defects in 2 of 11 eyes, both of which were early cases in our series. We believe that improved surgical technique allowed us to avoid such complications in later cases.[29,30] Because the induction of PVD in young eyes is particularly difficult, due to strong vitreoretinal adhesion, special care must always be taken to avoid excessive mechanical damage when separating the posterior hyaloid from the optic disc and posterior pole. A longer duration of surgery may also lead to an increased risk of light toxicity, as has been reported in macular hole surgery.[29–31] However, surgery-related insults must also be distinguished from VF aberrations that may be present preoperatively in these eyes with optic disc pits.

In conclusion, vitrectomy with modern surgical techniques for creating PVD in young patients and gas tamponade, without laser photocoagulation, can lead to successful reattachment of the macula and improvement in central vision in eyes with optic disc pit maculopathy, although most eyes required almost 1 year to reach this state.

## References


1. Wiethe T. Ein fall von angeborener Difformität der Sehnervenpapille. Arch Augenheilkd 1882;11:14–9.
2. Kranenburg EW. Crater-like holes in the optic disc and central serous retinopathy. Arch Ophthalmol 1960;64:912–24.
3. Brown GC, Shields JA, Goldberg RE. Congenital pits of the nerve head. II. Clinical studies in humans. Ophthalmology 1980;87:51–65.
4. Sobol WM, Blodi CF, Folk JC, Weingeist TA. Long-term visual outcome in patients with optic nerve pit and serous retinal detachment of the macula. Ophthalmology 1990;97:1539–42.
5. Lincoff H, Lopez R, Kreissig I, et al. Retinoschisis associated with optic nerve pits. Arch Ophthalmol 1988;106:61–7.
6. Rutledge BK, Puliafito CA, Duker JS, et al. Optical coherence tomography of macular lesions associated with optic nerve head pits. Ophthalmology 1996;103:1047–53.
7. Krivoy D, Gentile R, Liebmann JM, et al. Imaging congenital optic disc pits and associated maculopathy using optical coherence tomography. Arch Ophthalmol 1996;114:165–70.
8. Lincoff H, Kreissig I. Optical coherence tomography of pneumatic displacement of optic disc pit maculopathy. Br J Ophthalmol 1998;82:367–72.
9. Gass JDM. Serous detachment of the macula: secondary to congenital pit of the optic nervehead. Am J Ophthalmol 1969;67:821–41.
10. Gass JDM. Stereoscopic Atlas of Macular Diseases: Diagnosis and Treatment. Vol. II. 3rd ed. St. Louis: Mosby; 1987:728–33.
11. Tobe T, Nishimura T, Uyama M. Laser photocoagulation for pit-macular syndrome [in Japanese]. Ganka Rinshoiho 1991;85:124–30.

12. Cox MS, Witherspoon CD, Morris RE, Flynn HW. Evolving techniques in the treatment of macular detachment caused by optic nerve pits. Ophthalmology 1988;95:889–96.
13. Postel EA, Pulido JS, McNamara JA, Johnson MW. The etiology and treatment of macular detachment associated with optic nerve pits and related anomalies. Trans Am Ophthalmol Soc 1998;96:73–88.
14. Mitamura Y, Takeuchi S, Tsukahara I, et al. Vitreous surgery in two cases of pit-macular syndrome [in Japanese]. Rinsho Ganka 1997;51:251–4.
15. Snead MP, James N, Jacobs PM. Vitrectomy, argon laser, and gas tamponade for serous retinal detachment associated with an optic disc pit: a case report. Br J Ophthalmol 1991;75: 381–2.
16. Theodossiadis GP. Treatment of maculopathy associated with optic disk pit by sponge explant. Am J Ophthalmol 1996;121: 630–7.
17. Lincoff H, Yanuzzi L, Singerman L, et al. Improvement in visual function after displacement of the retinal elevations emanating from optic pits. Arch Ophthalmol 1993;111:1071–9.
18. Bonnet M. Serous macular detachment associated with optic nerve pits. Graefes Arch Clin Exp Ophthalmol 1991; 229:526–32.
19. Gordon R, Chatfield RK. Pits in the optic disc associated with macular degeneration. Br J Ophthalmol 1969;53:481–9.
20. Kelly NE, Wendel RT. Vitreous surgery for idiopathic macular holes. Results of a pilot study. Arch Ophthalmol 1991; 109:654–9.
21. Lewis H, Abrams GW, Blumenkranz MS, Campo RV. Vitrectomy for diabetic macular traction and edema associated with posterior hyaloidal traction. Ophthalmology 1992;99: 753–9.
22. Tachi N, Ogino N. Vitrectomy for diffuse macular edema in cases of diabetic retinopathy. Am J Ophthalmol 1996;122: 258–60.
23. Peyman GA, Cheema R, Conway MD, Fang T. Triamcinolone acetonide as an aid to visualization of the vitreous and the posterior hyaloid during pars plana vitrectomy. Retina 2000; 20:554–5.
24. Sakamoto T, Miyazaki M, Hisatomi T, et al. Triamcinolone-assisted pars plana vitrectomy improves the surgical procedures and decreases the postoperative blood-ocular barrier breakdown. Graefes Arch Clin Exp Ophthalmol 2002;240: 423–9.
25. Griffiths MFP. The use of fluorescein in vitrectomy [letter]. Arch Ophthalmol 1987;105:889.
26. Girard LJ. Fluorescein staining of formed vitreous to aid in vitrectomy [letter]. Ophthalmic Surg 1984;15:874.
27. Theodossiadis GP, Theodossiadis PA. Optical coherence tomography in optic disk pit maculopathy treated by the macular buckling procedure. Am J Ophthalmol 2001;132:184–90.
28. Michels RG, Thompson JT, Rice TA, Freund D. Effect of scleral buckling on vector forces caused by epiretinal membranes. Am J Ophthalmol 1987;104:667–70.
29. Pendergast SD, McCuen BW II. Visual field loss after macular hole surgery. Ophthalmology 1996;103:1069–77.
30. Ohji M, Nao-I N, Saito Y, et al. Prevention of visual field defect after macular hole surgery by passing air used for fluid-air exchange through water. Am J Ophthalmol 1999;127: 62–6.
31. Michels M, Lewis H, Abrams GW, et al. Macular phototoxicity caused by fiberoptic endoillumination during pars plana vitrectomy. Am J Ophthalmol 1992;114:287–96.

Available online at www.sciencedirect.com
SCIENCE DIRECT®
Experimental Eye Research 81 (2005) 751–758
EXPERIMENTAL EYE RESEARCH
www.elsevier.com/locate/yexer

# Physiological function of S-cone system is not enhanced in rd7 mice

Shinji Ueno[a], Mineo Kondo[a,*], Kentaro Miyata[a], Toshie Hirai[a], Takaki Miyata[b], Jiro Usukura[b], Yuji Nishizawa[b], Yozo Miyake[a]

[a]*Department of Ophthalmology, Nagoya University School of Medicine, 65 Tsuruma-cho, Showa-ku, Nagoya 466-8550, Japan*
[b]*Department of Anatomy and Cell Biology, Nagoya University School of Medicine, Nagoya 466-8550, Japan*

Received 2 October 2004; accepted in revised form 23 April 2005
Available online 11 July 2005

**Abstract**

The *rd7*mouse is a mutant mouse with a relatively late development of retinal degeneration. Earlier studies have shown that *rd7* mice have a distinctive pattern of retinal dysplasia with an increased number of cone cells, particularly those with S (short wavelength)-opsin immunoreactivity. These alterations of the *rd7* retina are caused by a mutation in the photoreceptor cell-specific nuclear receptor gene, *Nr2e3*, which is involved in the signaling pathway regulating photoreceptor cell differentiation, cell maintenance, and cell–cell interactions. The purpose of this study was to determine the physiological properties of the *rd7* retina using electroretinographic (ERG) techniques. We found that the maximal *a*-wave amplitude of the ERG in *rd7* mice was already reduced to half of the congenic controls at 6 weeks of age with normal phototransduction sensitivity. The photopic ERGs of *rd7* mice were not supernormal, and the amplitudes of the S-cone ERGs were not significantly different from those recorded in controls. These results suggested that even though the number of cones expressing S-opsin is increased, the physiological function of the S-cone system is not enhanced in *rd7* mice.


*Keywords:* electroretinogram; mouse; *Nr2e3*; *rd7*; retinal degeneration

## 1. Introduction

The *rd7* mouse is a mutant mouse with an autosomal recessive retinal degeneration (Chang et al., 1998; Akhmedov et al., 2000). There is a progressive degeneration of both the rod and cone systems, and ophthalmoscopy showed multiple white spots across the entire retina (Akhmedov et al., 2000). Histological examination demonstrated a distinctive pattern of dysplasia with waves, whorls, and rosettes in the outer nuclear layer (Chang et al., 1998; Akhmedov et al., 2000; Haider et al., 2001). Immunocytochemical studies showed that there was an increased number of cones, especially S (short-wavelength)-opsin expressing cone cells in the retina of *rd7* mice (Haider et al., 2001). These alterations of the retina resulted from a deletion of the photoreceptor cell specific nuclear receptor gene, *Nr2e3* (Akhmedov et al., 2000; Haider et al., 2001), which is known to be involved in the signaling pathway regulating photoreceptor cell differentiation, cell maintenance, and cell–cell interactions (Kobayashi et al., 1999; Haider et al., 2001; Yanagi et al., 2002).

In humans, mutations of the same *Nr2e3* gene were identified in patients with a unique type of retinal dystrophy called the enhanced S-cone syndrome (ESCS) (Haider et al., 2000). ESCS is an autosomal recessive retinal disorder which is characterized by night blindness, and an abnormally increased amplitude of the S-cone ERG (Marmor et al., 1990; Jacobson et al., 1990). Analysis of the electroretinograms (ERGs) in ESCS patients led to the hypothesis that there were more S-cones in the retina of these patients than in normals (Hood et al., 1995). Using imunocytochemical techniques on a postmortem retina, Milam et al. (2002) demonstrated that the number of cones was actually increased by approximately 2-fold, and 92% of these were S-cones. Thus, *Nr2e3* appeared to play an important role in the signaling pathway that controls the development and differentiation of this type of photoreceptor in both mice and humans.

The purpose of this study was to determine if these morphological alterations affected the physiological

* Corresponding author.
*E-mail address:* kondomi@med.nagoya-u.ac.jp (M. Kondo).

0014-4835/$ - see front matter © 2005 Elsevier Ltd. All rights reserved.
doi:10.1016/j.exer.2005.04.013

properties, including the S- and M-cone electroretinographic (ERG) responses, of the retina of *rd7* mice. We shall show that, contrary to our expectations, the *rd7* mice did not have enhanced S-cone responses despite the increased number of S-opsin expressing cone cells

## 2. Materials and methods

### 2.1. Animals

This study was conducted in accordance with the ARVO statement on the Use of Animals in Ophthalmic and Vision Research. Breeding pairs of *rd7* homozygous and congenic control (C57BL/6J) mice were obtained from Jackson Laboratory (Bar Harbor, Maine) and were bred in our laboratory. All mice were kept on a 12/12-hr light/dark cycle of fluorescent white light measuring 5 lux at cage level.

A total of 14 control mice and 14 *rd7* mice were used in this study. Twelve control and 12 *rd7* mice were used for ERG recordings. Two control and two *rd7* mice were used for both histological and immunohistochemical studies.

### 2.2. Fundus examination and histological analysis

Fundus photographs were taken with a fundus camera (Kowa, Nagoya, Japan). Histological analysis was performed as described previously (Hori et al., 2000). Semithin sections were cut along the vertical meridian through the optic nerve, and stained with hematoxylin and eosin.

### 2.3. Southern genotyping

Genomic DNA was extracted from tail snips of control mice and *rd7/rd7* homozygous mice using the phenol–chloroform method (Sambrook et al., 1989). The intron 5 fragment of *Nr2e3* gene was cloned as an RD7 probe by PCR amplification following TA cloning. The RD7 probe fragment was amplified using 100 ng of extracted control mouse tail DNA in 10.0 μl by PCR, The solution contained 10 pmol of forward (5′-GTTAACTCCCCGAGGAAAAGAT) and reverse (5′-TACCCAGGTTTTCAGATGTTCC) primers, 0.125 unit of LA-Taq (TAKARA BIO, Japan), 0.4 mM of dNTP, 1 × PCR buffer, and 2.5 mM $MgCl_2$. Ten of PCR reactions were subjected to the following cycling conditions: 94 °C for 1 min followed by 30 cycles of 94 °C for 30 sec, 58 °C for 30 sec, and 72 °C for 1 min, and a final extension of 72 °C for 5 min. The PCR product was electrophoresed on a 1% agarose gel, purified by QIA quick Gel Extraction Kit (QIAGEN), and cloned into pT7-blue vector (Novagen). The RD7 probe fragment was prepared by *Eco*RI and *Pst*I digestion from the cloned plasmid and purified with agarose gel electrophoresis and gel extraction as described above (Fig. 2A).

Genomic DNA from individual control mice and *rd7/rd7* homozygous mice were digested with BamHI, PstI and PvuII respectively, and probed with [32P]-labeled RD7 probe fragment. The wild-type and *rd7 Nr2e3* genes were identified by the following sized-band: 2.4 and 6.1 kb of BamHI blot, 1.1 and 3.0 kb of PstI blot, and 1.0 and 7.7 kb of PvuII blot.

### 2.4. Immunohistochemistry

Six-weeks-old mice were perfused transcardially with PLP fixative (McLean & Nakane, 1974), and the eyes were enucleated and postfixed in the same fixative for 60 min on ice. The eyes were then immersed in 20% sucrose, frozen in OCT compound (Sakura finetechnical Co., Ltd, Tokyo, Japan) and sectioned at 12 μm. Sections were blocked in 4% BSA in PBS and incubated with anti-blue opsin N-terminus peptide rabbit polyclonal antiserum (1:50 dilution) and Alexa Fluor 488 conjugated PNA (1:100, Invitrogen Corp., Carlsbad, CA, USA) for 2 hr. After washing with PBS, sections were incubated with Alexa Fluor 568 conjugated anti-rabbit IgG (1:100, Invitrogen Corp., Carlsbad, CA, USA). Specimens were examined with an epifluorescent microscope (BX60; Olympus).

### 2.5. Intensity-response functions of scotopic and photopic ERGs

After 12 hr of dark-adaptation, mice were anesthetized with an intramuscular injection of 80 mg/kg ketamine and 16 mg/kg xylazine and prepared for recordings under dim red light. Pupils were dilated with topical 0.5% tropicamide and 0.5% phenylephrine HCl, and the mice were placed on a heating pad for the duration of the ERG recordings.

ERGs were recorded with a gold wire loop placed on the cornea anesthetized with 1% tetracaine, and a drop of 1% methylcellulose to assure good contact. A gold wire electrode was placed on the sclera 1 mm from the temporal limbus as the reference electrode. The ground electrode was placed on the ear. Signals were amplified and bandpass filtered between 0.3 and 1000 Hz. The ERGs were averaged using a computer-assisted signal averaging system (Power Lab; AD Instruments, Castle Hill, Australia).

Scotopic ERGs were recorded with an interstimulus interval of 3–60 sec, and the interval increased with increasing stimulus intensity. The mice were placed in a Ganzfeld bowl (Model GS2000; LACE Electronica sel via Marmiccilo, Pisa, Italy), and 20–30 stroboscopic stimuli were averaged with a repetition rate of 1 sec to record the photopic ERGs. The maximum luminance was 1.0 log cd-s/$m^2$, and neutral density filters were used to reduce the stimulus intensity. Six equal stimulus intensity steps, ranging from −6.2 to 1.0 log cd-s/$m^2$, were used to elicit the scotopic ERGs, and four equal stimulus intensity steps, ranging from −0.8 to 1.0 log cd-s/$m^2$, were used to elict the photopic ERGs on a rod-desensitizing white adapting background of 1.3 log cd/$m^2$.

### 2.6. S-cone and M-cone ERG Recordings

The methods used for isolating the S- and M-cone ERG responses were essentially the same as those reported (Mears et al., 2001). Bright 1-ms stroboscopic stimuli (Model SB-28, Nikon, Tokyo, Japan) were used to elicit the ERGs. Narrow-band interference filters with $\lambda_{max}$ at 405 and 520 nm (nominal half-bandwidth, 10 nm) were used to elicit the short-wavelength sensitive and mid-wavelength sensitive systems. The stimuli were presented on a rod-desensitizing white adapting background of 1.3 log cd/m$^2$.

Initially, the intensities of the strobe luminance were adjusted to give approximately equal amplitude responses for both wavelengths in control mice of 6 months, and then these stimuli were used to assess the relative S-cone and M-cone responses in *rd7* mice.

## 3. Results

### 3.1. Fundus examination and histologic analysis

The fundus of *rd7* mice had a characteristic ophthalmoscopic appearance of multiple white spots across the entire retina, and the spots were more prominent at younger ages (Fig. 1A). Light microscopic examinations of retinal sections of *rd7* mice showed waves or whorls of the nuclei in the outer nuclear layer (Fig. 1B). These findings were the similar to those reported previously (Chang et al., 1998; Akhmedov et al., 2000).

### 3.2. Southern genotyping

The genomic organization and Southern genotyping of wild-type (top) and *rd7* (bottom) *Nr2e3* gene locus are shown in Fig. 2A. The RD7 probe and the BamHI (B), PstI (Ps), and PvuII (Pv) sites are indicated. The results of Southern-blot analysis of control (+/+) and *rd7/rd7* (−/−) mice are shown in Fig. 2B, and these blots demonstrated that *rd7/rd7*(−/−) mice lack the wild-type *Nr2e3* gene allele.

### 3.3. Immunohisotochemistry

The results of immunohistochemical analysis using peanut lectin (PNA) and blue opsin antibodies in *rd7* and control mice are shown in Fig. 3. It is clear that *rd7* mice have an increase in the number of S-opsin expressing cells as well as the total number of cone cells as reported (Haider et al., 2001). The results from the dorsal retina are shown in this figure, and the increases of S-opsin expressing cells and total cone cells are seen in both the ventral and dorsal retinas in *rd7* mice.

### 3.4. Scotopic and photopic ERGs

Representative scotopic ERGs elicited by increasing stimulus intensities from control and *rd7* mice at 6 weeks and 6 months of age are shown in Fig. 4A. Plots of the amplitude of the *a*- and *b*-waves as a function of stimulus intensity for both types of mice are shown in Fig. 4B. At 6 weeks of age, the amplitude of the *b*-wave in *rd7* mice was still preserved relatively well, and was reduced by appropriately 25% of the controls at the highest intensities. The amplitude of the *a*-wave, on the other hand, was reduced by about 50% of the control at this age (Fig. 4B, left half). As a result, the ratio of the *b*-wave to the *a*-wave amplitudes (*b/a* ratio) became larger in *rd7* mice than in control mice (Fig. 4A, left half). These results indicated that there was a retinal dysfunction at the levels of rod photoreceptor cells at a relatively young age of 6 weeks.

At 6 months of age the amplitudes of the *a*- and *b*-waves were reduced to about 35 and 40% of the controls, respectively (Fig. 4B, right half). These results indicated that there is progressive degeneration in the retina of *rd7* mice.

To determine if the rod phototransduction sensitivity is affected in rd7 mice, the kinetics of the *a*-waves of the *rd7* mice were compared to that of control mice. We did not use the *a*-wave fitting model of Lamb and Pugh (1992), but we assessed the time course of the *a*-wave elicited by a strong flash after normalization to the *a*-wave maximum amplitude (Hood and Birch., 1997; Pardue et al., 1998; Machida et al., 2000). Fig. 4C showed averaged ERG waveforms of six animals at 6 weeks of age elicited by 1.0 log cd-s/m$^2$.

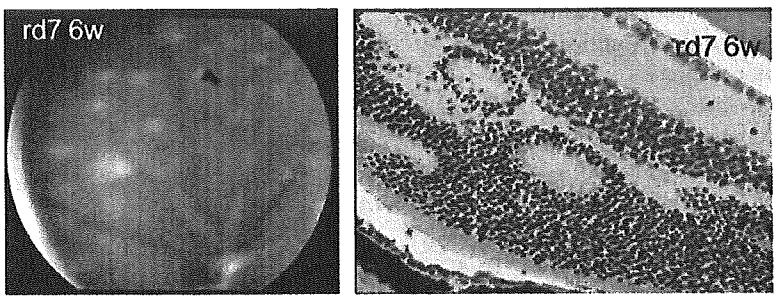


Fig. 1. Fundus photograph (A) and retinal histology (B) of a *6-week-old rd7* mouse.

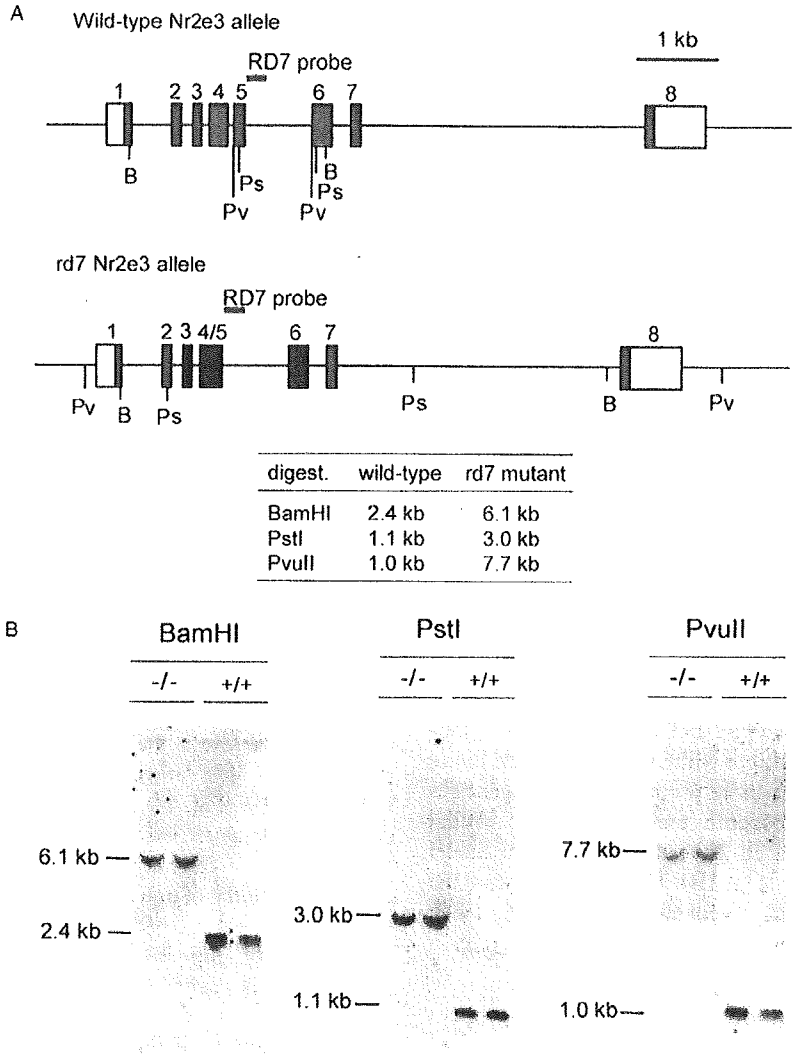


Fig. 2. Genetic defect in *Nr2e3* gene in *rd7* mice. (A) Genomic organization and Southern genotyping of wild-type (top) and *rd7* (bottom) *Nr2e3* gene locus. The RD7 probe and BamHI (B), PstI (Ps), and PvuII (Pv) sites are indicated. (B) Southern-blot analysis of control (+/+) and *rd7/rd7* (−/−) mice. *rd7/rd7* (−/−) mice lack wild-type *Nr2e3* gene allele.

The peak *a*-wave amplitude of *rd7* was normalized to that of the controls to compare the time course of the *a*-wave. When plotted in this manner, the leading edge of the *a*-wave overlapped completely for the two groups. These results suggested that rod phototransduction sensitivity is not altered in the *rd7* mice despite significantly reduced maximum rod photoreceptor responses.

Representative photopic ERGs elicited by increasing stimulus intensities from control and *rd7* mice at 6 weeks and 6 months are shown in Fig. 5A. Plots of the amplitude of the b-wave as a function of stimulus intensity for both types of mice are shown in Fig. 5B. At 6 weeks of age, the amplitude of the cone ERG *b*-wave was nearly the same as controls (Fig. 5B, left half). At 3 months of age, there was still no significant difference in the amplitude of cone ERG *b*-wave between control and *rd7* mice (data not shown). At 6 months of age, however, the *b*-wave amplitude in *rd7* became smaller than controls (about 80% at maximal intensity, Fig. 5B, right half), presumably due to the slow progression of retinal degeneration.

### 3.5. S- and M-cone ERGs

To determine whether the *rd7* mice had "enhanced" ERGs to short-wavelength stimuli, we recorded ERGs to monochromatic stimuli of 405 and 520 nm from control and *rd7* mice. Representative S- and M-cone ERGs from control and *rd7* mice at 6 weeks and 6 months of age are shown in Fig. 6A. The relative amplitude of the S-cone ERG to M-cone ERG did not differ between the *rd7* and control mice. The relative amplitude of the S-cone ERG to the M-cone ERG (S/M ratio) between two types of mice

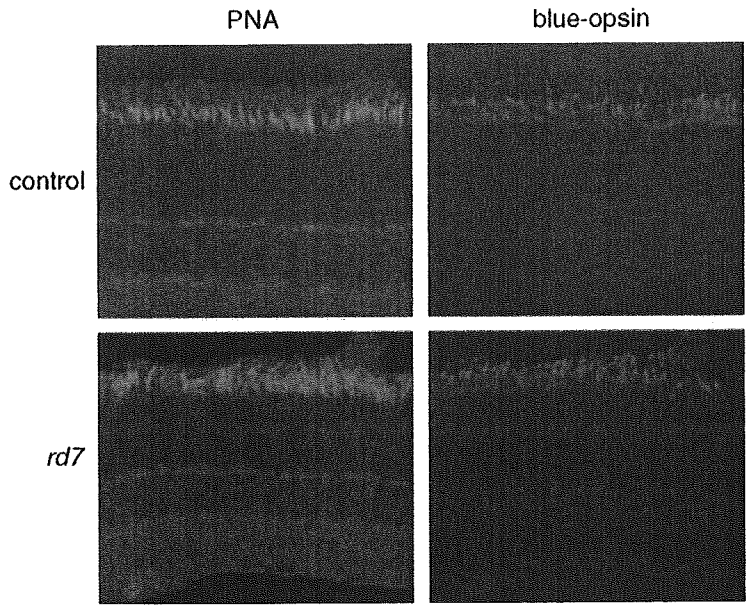


Fig. 3. Immunohisotochemistry of *rd7* and control mice retinal sections (dorsal retina) using PNA and blue opsin antibody. There is an increase in the number of S-cone cells as well as total cone cells in *rd7* mice.

are compared in Fig. 6B. The S/M amplitude ratio of the *rd7* tended to be slightly higher than controls at 6 weeks of age, but the difference was not statistically significant ($P=0.10$, Mann-Whitney's $U$ test). The difference in the S/M amplitude was also not significant at 6 months of age ($P=0.72$, Mann-Whitney's $U$ test).

## 4. Discussion

Our results demonstrated that the amplitude of the scotopic ERG a-wave in *rd7* mice was already reduced by about 50% of the controls at 6 weeks of age. These results are different from the results of Akhmedov et al. (2000), who reported that the ERGs of the *rd7* were within normal limits until 5 month of age. This difference is probably due to the different ERG recording conditions; Akhmedov et al. (2000) used relatively weak stimulus flashes which produce the *b*-waves as the main component, whereas we used white stimuli of different intensities which elicited the maximum a-wave amplitude. As shown in Fig. 4, the ERG abnormalities in the *rd7* are seen most clearly in the *a*-wave amplitudes elicited by high stimulus intensities.

At earlier ages, the *a*-waves of *rd7* mice were more impaired than the *b*-waves in the scotopic ERG. At this age, the amplitude of the scotopic ERG *b*-wave amplitude was relatively well preserved (75% of controls), whereas the *a*-wave amplitude was reduced by about 50% of the controls (Fig. 4, left half). This resulted in an increase in the *b/a* ratio. A similar phenomenon has been seen in other types of rodent models of retinal degeneration, e.g. the P23H rhodopsin transgenic rat (Machida et al., 2000; Aleman et al., 2001). The exact reason for such disproportional changes in the amplitude of *a*- and *b*-waves is still undetermined, but several hypotheses have been proposed, including the buffering by the large receptive fields of bipolar cells and synaptic remodeling following partial loss of rod photoreceptors (Machida et al., 2000; Aleman et al., 2001).

Haider et al. (2001) examined the retina of *rd7* mice using immunocytochemical techniques and reported that the number of cones (especially S-opsin immunoreactive cells) was 2-fold higher than in controls, which is in agreement with our data. However, our present ERG analysis showed that there was no significant difference in the amplitude of photopic ERGs between control and *rd7* mice. In addition, there was no statistically significant difference in the amplitude ratio of S-cone ERG to M-cone ERG between two types of mice. These discrepancies between the immunohistochemical and ERG findings are surprising and very interesting. One possible reason for the discrepancies is that even though the number of S-cone cell is increased, the S-cone system may not be functioning normally. It is known that there is a severe disorganization of the outer nuclear layer in the *rd7* retina, often showing waves, whorls, and rosettes (Chang et al., 1998; Akhmedov et al., 2000; Haider et al., 2001). Under such conditions, there must be some retinal dysfunction in the photon-catching ability, signal transduction, or synaptic transmission in the cone system of the *rd7* mice.

Finally, *rd7* mice are currently thought to be an animal model of human ESCS, because ESCS is caused by the mutations in the *Nr2e3* gene. However, our results indicate that there are at least two differences in

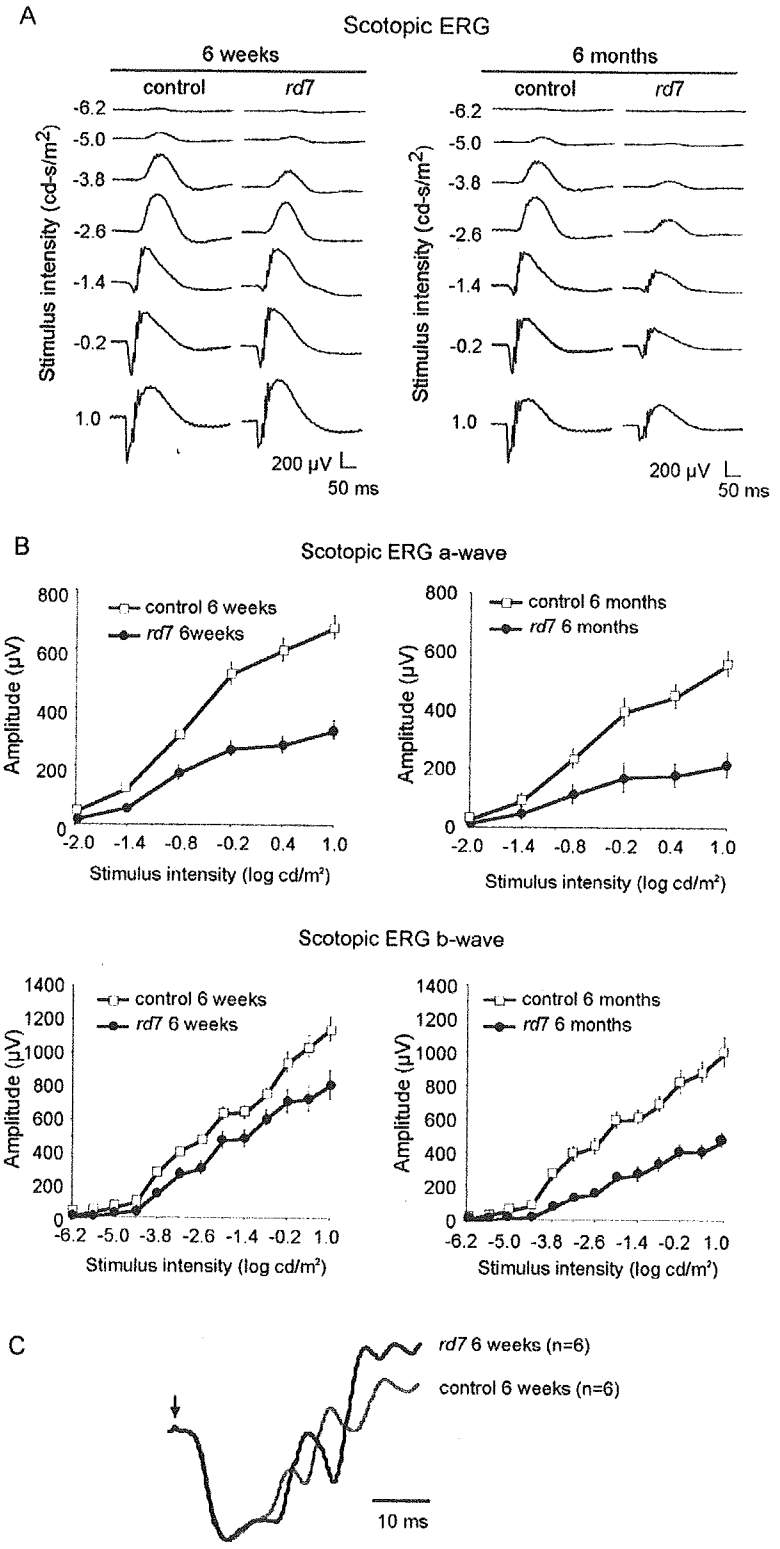


Fig. 4. (A) Representative scotopic ERGs elicited by different stimulus intensities for control and *rd7* mice at 6 weeks and 6 months of age. (B) Intensity-response functions of the scotopic ERGs for control and *rd7* mice at 6 weeks and 6 months of age. Means ± SEM of the amplitude obtained from six control and six *rd7* mice are plotted. (C) Averaged ERG waveforms of six animals of each 6-week-old rd7 (black line) and control mouse (gray line) elicited by 1.0 log cd-s/m$^2$. The peak a-wave amplitude of the rd7 mouse is normalized to that of the control to compare the time course of the *a*-wave.

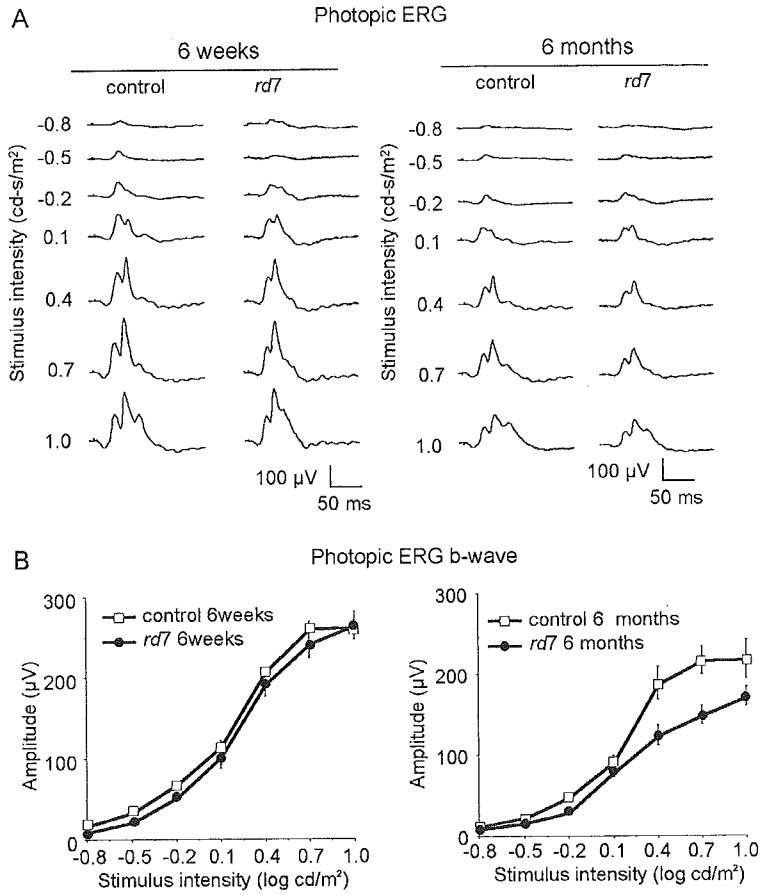


Fig. 5. (A) Representative photopic ERGs to various stimulus intensities for control and *rd7* mice at 6 weeks and 6 months of age. (B) Intensity-response functions of the photopic ERG for control and *rd7* mice at 6 weeks and 6 months of age. Means ± SEM of the amplitude obtained from six control and six *rd7* mice are plotted.

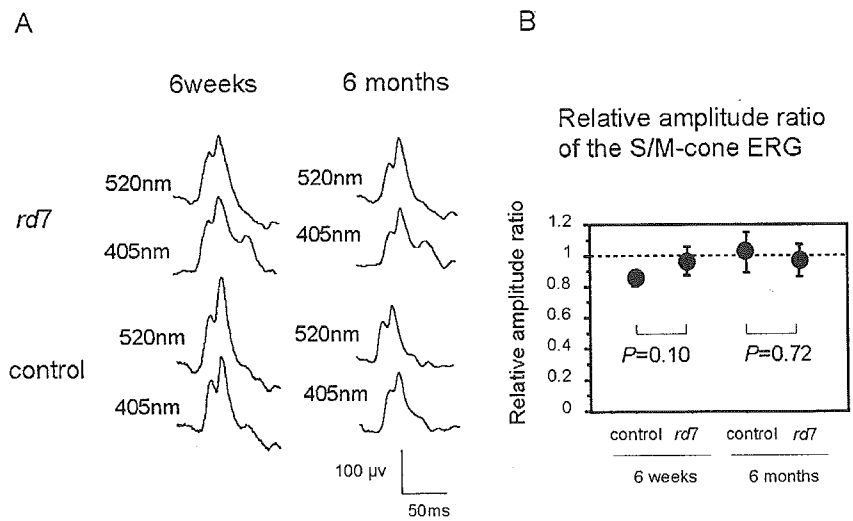


Fig. 6. S- and M-cone ERG responses. (A) Representative S- and M-cone ERGs recorded from control and *rd7* mice at 6 weeks and 6 months of age. (B) Relative amplitude ratio of the S-cone ERG to M-cone ERG for control and *rd7* mice at 6 weeks and 6 months of age. Means ± SEM of the relative amplitude ratio obtained from six control and six *rd7* mice are plotted.

the electrophysiology and phenotype between the human ESCS patients and *rd7* mice. First, *rd7* mice have some rod responses with normal phototransduction sensitivity (Fig. 4C), whereas human ESCS patients do not have detectable rod responses (Marmor et al., 1990; Jacobson et al., 1990). And second, *rd7* mice have normal S-cone ERG responses, whereas human ESCS patients have super normal S-cone ERGs (Jacobson et al., 1990; Hood et al., 1995). These phenotypic differences may be due to different types of mutations in the *Nr2e3* gene between the *rd7* mice and human ESCS or different species characteristics. In any cases, these properties in the *rd7* mice should be taken into consideration when one uses the *rd7* mice as an animal model of human ESCS.

## Acknowledgements

We thank Akira Shiota (YS INST. INC., Utsunomiya, Japan) for DNA analysis.

## References

Akhmedov, N.B., Piriev, N.I., Chang, B., Rapoport, A.L., Hawes, N.L., Nishina, P.M., Nusinowitz, S., Heckenlively, J.R., Roderick, T.H., Kozak, C.A., Danciger, M., Davisson, M.T., Farber, D.B., 2000. A deletion in a photoreceptor-specific nuclear receptor mRNA causes retinal degeneration in the *rd7* mouse. Proc. Natl Acad. Sci. USA 97, 5551–5556.

Aleman, T.S., LaVail, M.M., Montemayor, R., Ying, G., Maguire, M.M., Laties, A.M., Jacobson, S.G., Cideciyan, A.V., 2001. Augmented rod bipolar cell function in partial receptor loss: an ERG study in P23H rhodopsin transgenic and aging normal rats. Vision Res. 41, 2779–2797.

Chang, B., Heckenlively, J.R., Hawes, N.L., Davisson, M.T., 1998. A new mouse model of retinal dysplasia and degeneration (rd7). Invest. Ophthalmol. Vis. Sci. S880, 39 (Abstr.).

Haider, N.B., Jacobson, S.G., Cideciyan, A.V., Swiderski, R., Streb, L.M., Searby, C., Beck, G., Hockey, R., Hanna, D.B., Gorman, S., Duhl, D., Carmi, R., Bennett, J., Weleber, R.G., Fishman, G.A., Wright, A.F., Stone, E.M., Sheffield, V.C., 2000. Mutation of a nuclear receptor gene, NR2E3, causes enhanced S cone syndrome, a disorder of retinal cell fate. Nat. Genet. 24, 127–131.

Haider, N.B., Naggert, J.K., Nishina, P.M., 2001. Excess cone cell proliferation due to lack of a functional NR2E3 causes retinal dysplasia and degeneration in *rd7/rd7* mice. Hum. Mol. Genet. 10, 1619–1626.

Hood, D.C., Birch, D.G., 1997. Assessing abnormal rod photoreceptor activity with the a-wave of the electroretinogram: applications and methods. Doc. Ophthalmol. 92, 253–267.

Hood, D.C., Cideciyan, A.V., Roman, A.J., Jacobson, S.G., 1995. Enhanced S cone syndrome: evidence for an abnormally large number of S cones. Vision Res. 35, 1473–1481.

Hori, K., Katayama, N., Kachi, S., Kondo, M., Kadomatsu, K., Usukura, J., Muramatsu, T., Mori, S., Miyake, Y., 2000. Retinal dysfunction in basigin deficiency. Invest. Ophthalmol. Vis. Sci. 41, 3128–3133.

Jacobson, S.G., Marmor, M.F., Kemp, C.M., Knighton, R.W., 1990. SWS (blue) cone hypersensitivity in a newly identified retinal degeneration. Invest. Ophthalmol. Vis. Sci. 31, 827–838.

Kobayashi, M., Takezawa, S., Hara, K., Yu, R.T., Umesono, Y., Agata, K., Taniwaki, M., Yasuda, K., Umesono, K., 1999. Identification of a photoreceptor cell-specific nuclear receptor. Proc. Natl Acad. Sci. USA. 96, 4814–4819.

Lamb, T.D., Pugh Jr.., E.N., 1992. A quantitative account of the activation steps involved in phototransduction in amphibian photoreceptors. J. Physiol. 449, 719–758.

Machida, S., Kondo, M., Jamison, J.A., Khan, N.W., Kononen, L.T., Sugawara, T., Bush, R.A., Sieving, P.A., 2000. P23H rhodopsin transgenic rat: correlation of retinal function with histopathology. Invest. Ophthalmol. Vis. Sci. 41, 3200–3209.

Marmor, M.F., Jacobson, S.G., Foerster, M.H., Kellner, U., Weleber, R.G., 1990. Diagnostic clinical findings of a new syndrome with night blindness, maculopathy, and enhanced S cone sensitivity. Am. J. Ophthalmol. 110, 124–134.

McLean, I.W., Nakane, P.K., 1974. Periodate-Lysine-paraformaldehyde fixative. A new fixation for immunoelectron microscopy. J. Histochem. Cytochem. 22, 1077–1083.

Mears, A.J., Kondo, M., Swain, P.K., Takada, Y., Bush, R.A., Saunders, T.L., Sieving, P.A., Swaroop, A., 2001. Nrl is required for rod photoreceptor development. Nat. Genet. 29, 447–452.

Milam, A.H., Rose, L., Cideciyan, A.V., Barakat, M.R., Tang, W.X., Gupta, N., Aleman, T.S., Wright, A.F., Stone, E.M., Sheffield, V.C., Jacobson, S.G., 2002. The nuclear receptor NR2E3 plays a role in human retinal photoreceptor differentiation and degeneration. Proc. Natl Acad. Sci. USA. 99, 473–478.

Pardue, M.T., McCall, M.A., LaVail, M.M., Gregg, R.G., Peachey, N.S., 1998. A naturally occurring mouse model of X-linked congenital stationary night blindness. Invest. Ophthalmol. Vis. Sci. 39, 2443–2449.

Sambrook, J., Fritsch, E.F., Maniatis, T., 1989. Molecular cloning: A laboratory manual. Cold Spring Harbor Laboratory Press, Cold Spring Harbor.

Yanagi, Y., Takezawa, S., Kato, S., 2002. Distinct functions of photoreceptor cell-specific nuclear receptor, thyroid hormone receptor β2 and CRX in cone photoreceptor development. Invest. Ophthalmol. Vis. Sci. 43, 3489–3494.

# An Analog Silicon Retina With Multichip Configuration

Seiji Kameda and Tetsuya Yagi

*Abstract*—**The neuromorphic silicon retina is a novel analog very large scale integrated circuit that emulates the structure and the function of the retinal neuronal circuit. We fabricated a neuromorphic silicon retina, in which sample/hold circuits were embedded to generate fluctuation-suppressed outputs in the previous study [1]. The applications of this silicon retina, however, are limited because of a low spatial resolution and computational variability. In this paper, we have fabricated a multichip silicon retina in which the functional network circuits are divided into two chips: the photoreceptor network chip (P chip) and the horizontal cell network chip (H chip). The output images of the P chip are transferred to the H chip with analog voltages through the line-parallel transfer bus. The sample/hold circuits embedded in the P and H chips compensate for the pattern noise generated on the circuits, including the analog communication pathway. Using the multichip silicon retina together with an off-chip differential amplifier, spatial filtering of the image with an odd- and an even-symmetric orientation selective receptive fields was carried out in real time. The analog data transfer method in the present multichip silicon retina is useful to design analog neuromorphic multichip systems that mimic the hierarchical structure of neuronal networks in the visual system.**

*Index Terms*—**Analog VLSI, multichip, neuromorphic sensor, real time image processing, robot vision, silicon retina.**

## I. Introduction

THE visual information is processed by the retinal circuit following photo-transduction in the photoreceptors. The retinal circuit consists of several hierarchically arranged layers of neuronal syncytia that are relevant to lateral interactions among homogeneous type of neurons. Inspired by this unique architecture of the retinal circuit, neuromorphic silicon retinas, novel analog very large scale integrated (aVLSI) circuits, have been fabricated ([2]–[4] for outlines). The architecture of the neuromorphic chip becomes more complex to implement details of the retinal circuit [5], [6]. These neuromorphic chips, however, always encounter an intrinsic problem, namely, the tradeoff between the resolution and the computational complexity of the chip. Moreover, computations carried out on a single-chip are restricted, since the silicon retina computes an image with the physical properties of the built-in aVLSI circuit embedded on the chip. In the previous study, we fabricated a single-chip silicon retina that calculates spatial and temporal derivatives [1]. This silicon retina also encountered the same problem raised above, and, therefore, the applications of the silicon retina are confined. One of the feasible strategies to solve the problem, albeit only partially, is to divide the circuit into separate chips and carry out the computation in conjunction with simple off-chip circuits.

Manuscript received March 26, 2004; revised May 10, 2005.

S. Kameda was with the Department of Electronic Engineering, Graduate School of Engineering, Osaka University, Osaka 565-0871 Japan. He is now with the Graduate School of Advanced Sciences of Matter, Hiroshima University, Hiroshima, Japan (e-mail: kameda@dsl.hiroshima-u.ac.jp).

T. Yagi is with the Department of Electronic Engineering, Graduate School of Engineering, Osaka University, Osaka 565-0871, Japan (e-mail: yagi@ele.eng.osaka-u.ac.jp).

Digital Object Identifier 10.1109/TNN.2005.860867

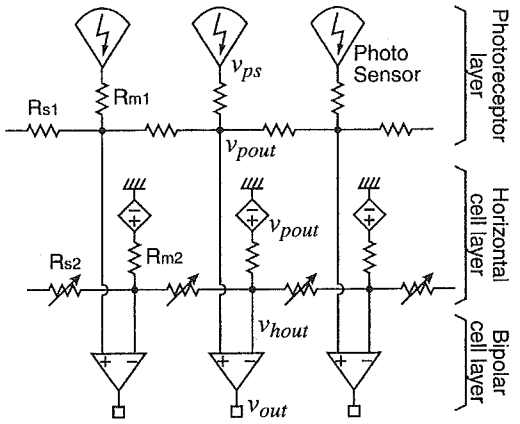


Fig. 1. Outer retinal circuit model. The model consists of two resistive network layers and a differential amplifier layer. In the vertebrate retina, the first and second resistive networks represent a photoreceptor and horizontal cell layers, respectively. The differential amplifier layer represents a bipolar cell layer and takes the difference between two resistive networks. The receptive field is approximated by the $\nabla^2 G$ filter.

In previous studies, the multichip systems have been fabricated [7]–[13]. In these multichip systems, high resolution and advanced functions are realized using the address event representation (AER) for data transfer between chips [14]–[17]. The AER preserves the continuous time nature of neural processing in the brain, and is advantageous in terms of low power communication.

In this paper, we have fabricated a multichip silicon retina, in which the functional network circuits are divided and fabricated in separate chips. These separate chips are linked by a line-parallel transfer bus and communicate with analog signals under conditions of synchronous discrete time sampling. The analog image transfer method employed in the present multichip is thought to be suitable to engineering applications with regard to compatibility with the conventional image processing systems. Using the multichip silicon retina in combination with an off-chip differential amplifier under a control by field programmable gate array (FPGA) logic, even- and odd-symmetric orientation selective filterings were carried out in real time.

## II. Multichip Silicon Retina

The outer retinal circuit consisting of the photoreceptor, the horizontal cell and the bipolar cell, has been described as a two layers of resistive network [18], [19] as shown in Fig. 1. In

Fig. 1, the first resistive network represents the photoreceptor layer, and the second one represents the horizontal cell layer of the vertebrate retina. Each resistive network has a different tightness of electrical coupling between neighboring nodes. In our previous study, this network model was fabricated on a single-chip [1]. In this paper, each resistive network was fabricated on a separate chip. By being fabricated in such a way, the spatial resolution of the chip can be increased and more flexible computations can be carried out as will be shown later.

The previously fabricated single-chip silicon retina emulates the sustained and transient responses found in the vertebrate retina [1]. The single-chip silicon retina, however, includes two layers of resistive networks and two arrays of sample/hold (S/H) circuits, besides the photo sensors. Therefore, the circuits following the photo sensors occupy a significant chip area, which limits the fill factor and resolution. To overcome this problem, the circuits embedded in the single-chip were divided and fabricated into two separate chips: a photoreceptor network chip and a horizontal cell network chip. The photoreceptor network chip (P chip) corresponds to the first resistive network and the horizontal cell network chip (H chip) corresponds to the second resistive network.

### A. Circuit Designs

Fig. 2(A) shows the circuit design depicting a single pixel of the P chip. In the P chip, an image is obtained by the photo sensors. The photo sensor is an active pixel sensor (APS) that consists of a standard n+/Psub photo-diode and a source-follower circuit [20], [21]. The APS has a high sensitivity to light, by accumulating the photoelectron in the parasitic capacitor of the photo-diode. A dynamic range of the photo sensor can be controlled by changing the accumulation time. The image is smoothed by a resistive network that corresponds to the first resistive network of the previous single-chip silicon retina. The resistive network consists of a MOS resistor [3], [22]. Fig. 2(B) shows the detailed design of the resistive network. The resistances of MOS resistors can be controlled by external bias voltages ($V_{\rm bm1}$, $V_{\rm bs1}$, $V_{\rm bm2}$, and $V_{\rm bs2}$), and the variable range of the resistance depends on the PMOS transistor aspect ratio W/L. The extent of smoothing can be controlled by external bias voltages applied to the MOS resistors, and the variable range of smoothing is determined by the ratio between the resistances of the $\rm R_{m1}$ and $\rm R_{s1}$. The S/H circuits, Nbuf1, consists of a wide range amplifier [Fig. 2(C)] and two capacitors, and is embedded to compensate for the circuit offsets, namely, the amplifier offset and the fixed pattern noise due to the statistical mismatch of transistor characteristics [23], [24]. The offset compensation on each chip is indispensable to the multichip silicon retina. A current applied to the amplifier is about 10 $\mu$A, which comprises a large percentage of a current applied to the pixel circuit in order to speed up a read time of output voltages.

Fig. 3(A) shows a circuit design depicting a single pixel of the H chip. The input to the H chip pixel from the corresponding P chip pixel, $v_{\rm hi}$, is stored in an analog memory (AMem). Fig. 3(B) shows the detailed design of the analog memory, which consists of a capacitor and a voltage follower with a transconductance amplifier [3]. The stored voltage is smoothed by the resistive network of the H chip, corresponding

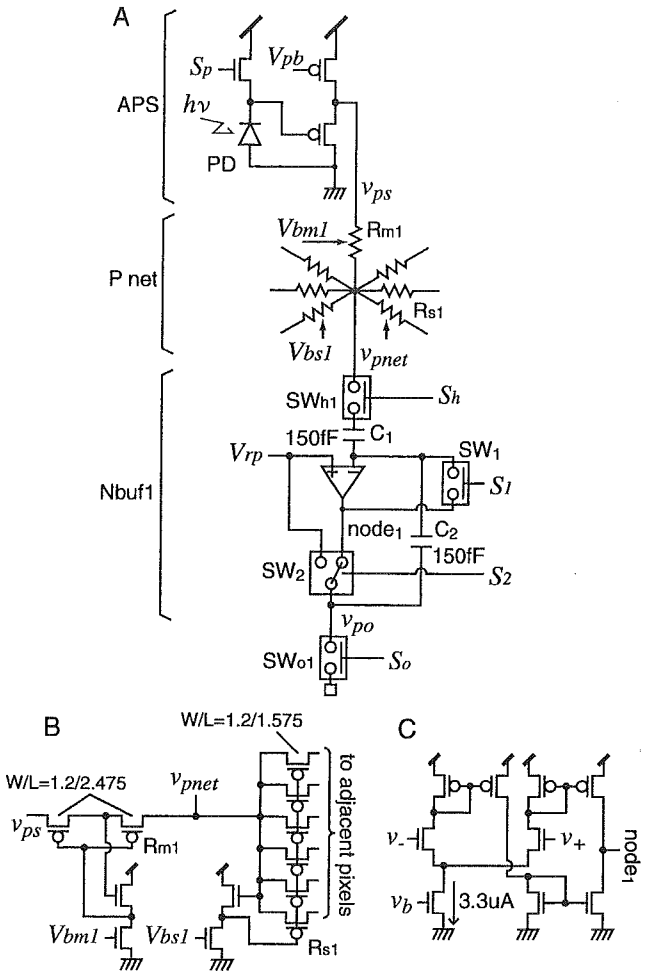


Fig. 2. A: Circuit design depicting the single pixel of the photoreceptor network chip (P chip). The pixel circuit consists of a photo sensor (APS), a resistive network (P net), and a S/H circuit (Nbuf1). B: Detailed design of the P net. The P net is controlled separately by two MOS resistors, $\rm R_{m1}$ and $\rm R_{s1}$. Therefore, an extent of smoothing is controlled by bias voltages, $V_{\rm bm1}$ and $V_{\rm bs1}$. C: Detailed design of a wide range amplifier of the Nbuf1 [3]. A current applied to the amplifier is about 10 mA. A transmission gate is used on each of the switches, $\rm SW_x$.

to the second resistive network of the single-chip silicon retina. Fig. 3(C) shows the detailed design of the resistive network. The extent of smoothing is controllable by external bias voltages ($V_{\rm bm2}$, $V_{\rm bs2x}$, $V_{\rm bs2y}$, and $V_{\rm bs2z}$). Note that the electrical coupling can be modulated in one of three orientations since the bias voltages ($V_{\rm bs2x}$, $V_{\rm bs2y}$, and $V_{\rm bs2z}$) are controlled independently. The variable range of smoothing of the H chip is larger than that of the P chip. S/H circuits, which are the same as the P chip, compensate for the pattern noise generated on the transfer bus as well as the circuit offsets of the H chip.

Fig. 4 illustrates a block diagram depicting the pixel arrangement of the P and H chips. In the P chip, the photo-diodes (PD: shadowed squares) are arranged on a hexagonal grid for better circular symmetry, as well as for better spatial sampling efficiency compared to a square grid [3], [25]. The output of a pixel selected by the vertical and the horizontal shift registers (VSR and HSR) is read out successively: the outputs of P chip pixels are transferred to the H chip using a line parallel method, in which the outputs of the pixels in the same row are read out and